Prediction and Identification of Drug Interactions with the Human ATP-Binding Cassette Transporter Multidrug-Resistance Associated Protein 2 (MRP2; ABCC2)

Jenny M. Pedersen,[†,‡] Pär Matsson,[†,‡] Christel A. S. Bergström,[†] Ulf Norinder,[†,§] Janet Hoogstraate,[§] and Per Artursson[†,*]

Pharmaceutical Screening and Informatics, Department of Pharmacy, Uppsala University, Biomedical Center, Post Office Box 580, SE-751 23 Uppsala, Sweden, Department of Medicinal Chemistry, AstraZeneca R&D Södertälje, SE-151 85 Södertälje, Sweden

Received December 14, 2007

The chemical space of registered oral drugs was explored for inhibitors of the human multidrug-resistance associated protein 2 (MRP2; ABCC2), using a data set of 191 structurally diverse drugs and drug-like compounds. The data set included a new reference set of 75 compounds, for studies of hepatic drug interactions with transport proteins, CYP enzymes, and compounds associated with liver toxicity. The inhibition of MRP2-mediated transport of estradiol-17β-D-glucuronide was studied in inverted membrane vesicles from Sf9 cells overexpressing human MRP2. A total of 27 previously unknown MRP2 inhibitors were identified, and the results indicate an overlapping but narrower inhibitor space for MRP2 compared with the two other major ABC efflux transporters P-gp (ABCB1) and BCRP (ABCG2). In addition, 13 compounds were shown to stimulate the transport of estradiol-17β-D-glucuronide. The experimental results were used to develop a computational model able to discriminate inhibitors from noninhibitors according to their molecular structure, resulting in a predictive power of 86% for the training set and 72% for the test set. The inhibitors were in general larger and more lipophilic and presented a higher aromaticity than the noninhibitors. The developed computational model is applicable in an early stage of the drug discovery process and is proposed as a tool for prediction of MRP2-mediated hepatic drug interactions and toxicity.

Introduction

Efflux transporters from the ATP-binding cassette (ABC[a]) transporter family are major determinants of drug disposition that limit the uptake of drugs in target cells and over tissue barriers such as the intestinal epithelium and blood−brain barrier. These transporters also mediate secretion of drug metabolites, for instance, into bile and urine.[1] Multidrug-resistance associated protein 2 (MRP2/ ABCC2) is one of the most extensively expressed ATP-binding cassette (ABC) transporters in the human liver[2–4] and is a major determinant of the biliary efflux of intrinsically anionic drugs such as methotrexate[5] and pravastatin,[6] as well as anionic conjugates of drugs and endogenous compounds.[7]

The primary endogenous role of MRP2 is to mediate biliary efflux of conjugated bile salts and drugs as part of the hepatic detoxification process; genetic disorders resulting in nonfunctional MRP2 give rise to Dubin−Johnson syndrome, a conjugated hyperbilirubinemia.[8] Furthermore, inhibition of MRP2 in the hepatocyte can result in disruption of the lipid homeostasis and toxic accumulation of compounds in the liver, which is a major cause of withdrawal of drugs from the market.[9–11] This effect is likely to be more prominent in patients where MRP2-mediated transport is genetically or pharmacologically impaired.[12,13]

Apart from a few studies on limited series of structurally related drug molecules,[14–17] the molecular determinants of drug-mediated MRP2 inhibition are largely unexplored. This is probably because ABC transporters such as MRP2 are integral membrane proteins, and high-resolution crystal structures of most of these have still not been described.[18–20] Also, studies of drug affinity for MRP2 are complicated by the possible existence of several drug binding sites in this protein.[21,22]

In this investigation, a data set of 191 compounds covering the chemical space of registered oral drugs was studied for MRP2 inhibition. The data set included a new reference set of 75 compounds for studies of drug interactions with common hepatic transport proteins and CYP enzymes as well as assessing liver-mediated toxicity. The identified inhibitors were larger, more lipophilic and presented more aromatic features than the noninhibitors. An easily interpreted computational model was also developed that successfully discriminates inhibitors from noninhibitors based on these molecular properties.

Results

MRP2 Inhibition Assay. The rate of ATP-dependent estradiol-17β-D-glucuronide ($E_{17}G$) transport into MRP2-overexpressing inverted membrane vesicles was linear for up to 30 min (Figure 1A), during which time transport into control vesicles incubated with AMP was negligible (~0.25%). The rate of $E_{17}G$ transport was sigmoidally related to the substrate concentration (Figure 1B), indicating that $E_{17}G$ stimulates its own transport.[21,22] The transport kinetics were determined from Figure 1B using nonlinear regression, resulting in an apparent K_m of 94 ± 7 μM. This is in agreement with previous results in corresponding membrane vesicles.[22] The maximum transport

* To whom correspondence should be addressed. Telephone: +46 18 471 44 71. Fax: +46 18 471 44 84. E-mail: per.artursson@farmaci.uu.se.
† Uppsala University.
‡ Contributed equally to this paper.
§ AstraZeneca R&D Södertälje.

[a] Abbreviations: ABC, ATP-binding cassette transporter; BCRP, breast cancer resistance protein (ABCG2); BSEP, bile salt export pump (ABCB11); CYP, cytochrome P450; DMSO, dimethyl sulfoxide; hERG, human ether-a-go-go ion chanel; logD7.4, octanol–water partition coefficient at pH 7.4; MATE, multidrug and toxin extrusion transporter; MCT, monocarboxylate transporter; MRP2, multidrug resistance associated protein 2 (ABCC2); OAT, organic anion transporter; OATP, organic anion transporting polypeptide; OCT, organic cation transporter; P-gp, P-glycoprotein (ABCB1); OPLS-DA, orthogonal partial least-squares projection to latent structures discriminant analysis; SLC, solute carrier.

10.1021/jm7015683 CCC: $40.75
Published on Web 05/06/2008

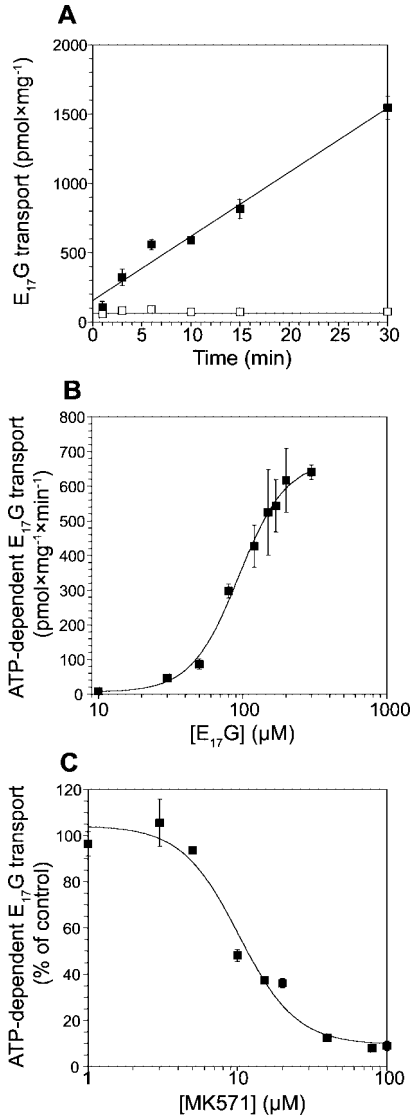

Figure 1. (A) $E_{17}G$ transport in MRP2-overexpressing inverted membrane vesicles. The $E_{17}G$ transport was linear up to 30 min. The influence of passive diffusion was negligible (<0.25%), as determined in membrane vesicles incubated with AMP instead of ATP. Closed squares denote the $E_{17}G$ transport in membrane vesicles incubated with ATP, and open squares denote the transport in AMP-incubated membrane vesicles. The data are presented as means ± SE ($n = 3$). (B) $E_{17}G$ transport kinetics in MRP2-expressing membrane vesicles. The ATP-dependent transport rates were calculated by subtracting the initial transport rate in vesicles incubated with AMP from that obtained in ATP-incubated vesicles. K_m was 94 ± 7 μM, V_{max} was 680 ± 30 pmol × mg protein^{-1} × min^{-1}, and the Hill coefficient was 2.6. (C) Inhibition of ATP-dependent $E_{17}G$ transport by increasing concentrations of the MRP inhibitor MK571 ($IC_{50} = 10 \pm 1.5$ μM). Intravesicular $E_{17}G$ was detected by scintillation counting after a 10 min incubation. The data are presented as means ± SE ($n = 3$).

rate (V_{max}) was 680 ± 30 pmol × min^{-1} × mg protein^{-1}, and the Hill coefficient was 2.6, suggesting the existence of at least two substrate binding sites in the MRP2 protein, which is in agreement with previous studies.[22]

Coincubation of the membrane vesicles with 50 μM $E_{17}G$ and 80 μM of the MRP inhibitor MK571[23] resulted in complete inhibition of $E_{17}G$ transport (Figure 1C; $IC_{50} = 10 \pm 1.5$ μM). The reduction in transport rate was caused by specific inhibition of the ATP-dependent $E_{17}G$ transport; no effect on passive transport was observed (data not shown).

Inhibition and Stimulation of MRP2-Mediated Estradiol-17β-D-glucuronide Transport. A standard inhibitor concentration of 80 μM was selected to be in the vicinity of the $E_{17}G$ apparent K_m of 94 μM. At this concentration, the ATP-dependent MRP2-mediated transport was inhibited by 50% or more by 42 (22%) of the 191 test compounds (Table 1, Figure 2).

The inhibitors were spread across several chemical and therapeutical classes, including antivirals (saquinavir, ritonavir, and lopinavir), cytostatics (erlotinib and tamoxifen), and antipsycotic agents (thioridazine, flupenthixol, and chlorprothixene).

Our experimental protocol was designed to reveal MRP2 inhibitors, with less emphasis on stimulation of transport, as described in the Materials and Methods. Nevertheless, 13 (7%) of the compounds in the data set significantly increased the $E_{17}G$ transport (Table 1, Figure 2). Seven new stimulators were identified, corresponding to 54% of the identified stimulating compounds (Table 1). The higher $E_{17}G$ concentration used in this investigation than in studies focused on transport stimulation suggests that the stimulators identified here are relatively potent.

Important Molecular Features for MRP2 Inhibition. The inhibitors differed significantly in structure from the noninhibitors in that they were on average larger (molecular weight, Figure 3A) and exhibited more prominent lipophilic (octanol–water partition coefficient, Figure 3B) and hydrophobic characteristics (surface area of nonpolar atoms, Figure 3C). The inhibitors were also shown to have higher aromaticity than the noninhibitors (surface area of unsaturated nonpolar atoms, Figure 3D). In contrast, the surface area of polar atoms (PSA, Figure 3E) and the charge (Figure 3F) were similar in both groups. However, as expected, the overlap between inhibitors and noninhibitors was too large to allow adequate discrimination between the two groups based on a single molecular descriptor. Rule-based decision tree models were also not able to successfully discriminate between the groups (data not shown).[24]

To better define the molecular features important for the binding of inhibitors to MRP2, we developed a multivariate OPLS-DA model that distinguishes between MRP2 inhibitors and noninhibitors. After stepwise exclusion of molecular descriptors with insignificant influence on the discriminating model, the initial set of 240 descriptors was condensed to the five that were most important (Figure 4A). The coefficients in the final model show that a combination of increased lipophilicity, aromaticity, and size are major determinants for the MRP2 inhibitory effect, supporting the results from the single-descriptor analysis.

The model successfully classified 86% of both MRP2 inhibitors and noninhibitors in the training set. The structurally diverse test set was used to confirm the ability of the OPLS-DA model to predict inhibition and resulted in correct classifications for 72% of the MRP2 inhibitors and 71% of the noninhibitors (Figure 4B), which is comparable to similar models for other transport proteins, such as P-gp (ABCB1)[25,26] and BCRP (ABCG2).[27] Interestingly, despite the fact that the model was based on a binary classification of the experimental data (inhibitor/noninhibitor), 75% of the eight compounds falsely predicted as noninhibitors (morin, quercetin, baicalin, *p*-aminohippuric acid, lisinopril, and isradipine) have experimental values close to the selected cutoff value of 50% inhibition. This suggests that the molecular descriptors also encode some information about the relative potency of the inhibitors and indicates that the risk of the model describing chance correlations is very small.

Table 1. Identification of MRP2 Inhibitors and Stimulators among the 191 Compounds in this Study[a]

	substance	relative transport rate[b] (% of control)	$logD_{7.4}$[c]	MW[d] g × mol^{-1}	PSA[e] Å^2
negative control	n.a.[f]	100 ± 11	n.a.	n.a.	n.a.
inhibitors	thioridazine[g]	−1 ± 2	4.5	371	9
	terfenadine[g]	3 ± 1	5.9	472	38
	fendiline[g,h]	5 ± 1	3.6	315	12
	bromosulfalein	5 ± 2	0.4	794	189
	glycyrrhizinic acid[h]	5 ± 1	0.5	823	268
	indocyanine green	5 ± 3	4.6	754	131
	loratadine[g]	6 ± 1	4.5	383	35
	5-CFDA[g]	7 ± 3	0.4	460	141
	tamoxifen[g,h]	8 ± 1	5.0	372	18
	MK571[h]	9 ± 3	1.9	515	73
	Fluo-3	9 ± 2	0.5	770	247
	benzbromarone	11 ± 1	4.0	424	50
	diethylstilbestrol[g,h]	11 ± 1	4.6	268	47
	silymarin[g]	14 ± 13	1.5	482	171
	clotrimazole[g]	14 ± 4	5.0	345	15
	rifampicin[g]	18 ± 5	1.9	823	190
	chlorprothixene[g]	25 ± 6	4.3	316	7
	taurolithocholic acid[g]	27 ± 4	2.1	484	118
	ivermectin[g]	28 ± 4	5.5	875	152
	lopinavir[g,h]	33 ± 12	5.2	629	89
	lansoprazole[h]	34 ± 10	2.0	369	70
	baicalin[h]	34 ± 5	−2.3	446	194
	astemizole[g,h]	36 ± 10	5.4	459	41
	reserpine	37 ± 4	3.3	609	103
	GF120918[h]	39 ± 8	4.6	564	93
	quercetin[g,h]	40 ± 8	1.0	302	137
	cyclosporine-A	40 ± 7	4.5	1203	210
	diltiazem[g]	40 ± 13	2.4	415	60
	saquinavir	41 ± 6	4.6	671	139
	dipyridamole[g,h]	42 ± 13	1.5	505	121
	chelerythrine	43 ± 8	2.6	348	51
	lisinopril[g]	43 ± 12	−4.1	405	134
	sanguinarine chloride[g]	44 ± 7	2.2	332	55
	flupentixol[g]	46 ± 7	3.7	435	35
	p-aminohippuric acid[h]	46 ± 11	−4.2	194	99
	loperamide[g]	46 ± 7	4.8	477	41
	fenofibrate[g,h]	46 ± 10	5.0	361	53
	isradipine[g]	46 ± 10	3.3	371	101
	celecoxib[g]	46 ± 11	3.4	381	82
	erlotinib[g]	47 ± 7	3.3	393	78
	ritonavir	48 ± 4	4.3	721	106
	morin[g]	50 ± 8	0.8	302	136
borderline inhibitors	amitriptyline	51 ± 4	3.1	277	7
	prednisone	51 ± 5	1.6	358	91
	ranitidine	52 ± 6	0.7	314	87
	ethinylestradiol	53 ± 11	3.7	296	43
	tinidazole	55 ± 6	−0.4	247	101
	verapamil	56 ± 11	3.7	455	80
	nystatin	56 ± 5	−2.1	926	279
	maprotiline	56 ± 12	2.3	277	16
	dextromethorphan	57 ± 10	2.2	271	19
	desipramine	57 ± 7	1.8	266	17
	propafenone	58 ± 11	1.6	341	61
	chlorpromazine	58 ± 14	3.9	319	9
	atropine	59 ± 15	0.8	289	47
	nicardipine	59 ± 12	4.4	480	122
	ergocristine	60 ± 8	4.4	610	102
	amodiaquine	60 ± 9	3.6	356	51
	simvastatin	61 ± 11	4.6	419	73
	procyclidine	62 ± 14	2.6	287	21
	cefamandole	63 ± 7	−3.3	463	168
	quinidine	64 ± 6	2.4	324	51
	amiodarone	66 ± 5	4.8	645	42
	tryptophan	66 ± 15	−3.6	204	81
	cefadroxil	68 ± 7	−4.9	363	132
	pramoxine	69 ± 11	2.7	293	43
	propranolol	69 ± 9	1.2	259	45
	hoechst 33342	70 ± 16	3.1	453	77
	fusidic acid	72 ± 8	3.0	517	95
	metoprolol	72 ± 7	0.2	267	60
	1-methyl-4-phenylpyridinium	72 ± 13	0.5	170	3
	flucloxacillin	73 ± 9	−0.5	454	120

Table 1. Continued

	substance	relative transport rate[b] (% of control)	$logD_{7.4}$[c]	MW[d] g × mol^{-1}	PSA[e] Å^2
	Ko143	73 ± 17	3.6	470	87
	gefitinib	74 ± 15	4.4	447	74
	imatinib mesylate	74 ± 9	2.5	494	79
	chlorzoxazone	74 ± 11	1.8	170	51
	tyrphostin	75 ± 11	1.6	448	197
	quinine	75 ± 10	2.4	324	51
	resveratrol	75 ± 8	2.9	228	71
	benzylpenicillin	76 ± 15	−1.3	334	95
	ketoconazole	76 ± 6	4.1	531	74
	sulfasalazine	77 ± 11	1.3	398	136
	prazosin	78 ± 15	1.6	383	102
	vinblastine	78 ± 15	4.5	811	116
	noscapine	78 ± 17	1.9	413	88
noninhibitors	glipizide[h]	81 ± 8	0.7	446	128
	5-carboxyfluorescein	82 ± 7	0.6	376	130
	vincristine	82 ± 18	4.2	825	136
	amiloride	82 ± 18	−3.3	230	150
	phenacetin	83 ± 14	1.6	179	42
	ofloxacin	83 ± 12	−3.0	361	84
	carnitine[h]	84 ± 4	−3.0	162	57
	antipyrine	84 ± 17	1.3	188	27
	biochanin A	84 ± 5	2.8	284	85
	carbamazepine[h]	86 ± 17	2.4	236	44
	felodipine	86 ± 20	4.9	384	68
	ritanserin	86 ± 17	5.4	478	38
	taurocholate[h]	87 ± 16	0.1	516	150
	doxorubicin	87 ± 15	0.2	544	194
	phenformin	88 ± 10	−2.5	205	96
	tipranavir	88 ± 14	5.0	603	101
	erythromycin[h]	89 ± 8	3.1	734	124
	tramadol[h]	89 ± 8	1.0	263	31
	timolol	91 ± 11	0.1	316	84
	cimetidine[h]	91 ± 11	0.2	252	89
	naproxen	92 ± 2	0.5	230	54
	rotenone	92 ± 12	3.6	394	73
	indinavir[h]	93 ± 10	4.6	614	100
	seglitide[h]	94 ± 9	0.8	809	190
	terazosin	94 ± 22	1.6	387	107
	hydrochlorothiazide[h]	94 ± 13	−0.3	298	131
	valproic acid[h]	94 ± 18	0.3	144	36
	valacyclovir[h]	94 ± 12	−3.1	324	153
	apigenin	94 ± 9	2.3	270	95
	nitrofurantoin	94 ± 15	−0.6	238	139
	phenylethyl isothiocyanate	94 ± 8	3.7	163	13
	adefovir[h]	96 ± 18	−5.5	273	149
	isoniazid	96 ± 10	−0.6	137	73
	sotalol	96 ± 22	−1.5	272	84
	fexofenadine[h]	97 ± 13	2.4	502	79
	phenobarbital[h]	98 ± 11	1.4	232	88
	tranilast	98 ± 6	1.8	327	89
	4-nitrophenyl glucuronide	99 ± 19	−3.3	315	173
	digoxin[h]	99 ± 13	2.4	781	200
	piroxicam	100 ± 17	0.2	331	93
	nicotine	101 ± 13	0.2	162	18
	colchicine	101 ± 8	1.8	399	89
	N-methylnicotinamide[h]	101 ± 21	0.0	136	43
	omeprazole[h]	101 ± 9	1.6	345	83
	amantadine	101 ± 20	−0.4	151	26
	chenodeoxycholic acid	101 ± 13	2.7	393	85
	irinotecan[h]	101 ± 23	3.0	587	116
	genistein	101 ± 6	2.2	270	96
	chloroquine[h]	102 ± 14	2.0	320	26
	oxazepam	103 ± 18	2.3	287	65
	leucovorin[h]	103 ± 11	−6.6	473	225
	zidovudine	103 ± 28	−0.2	267	135
	captopril	104 ± 15	−2.2	217	60
	disopyramide	104 ± 20	1.9	339	56
	haloperidol	106 ± 9	3.2	376	40
	bupropion	106 ± 16	2.1	240	29
	nandrolone	106 ± 9	2.7	274	42
	trimethoprim	107 ± 16	1.3	290	109
	flurbiprofen	108 ± 13	0.8	244	41
	taxifolin[h]	108 ± 10	0.5	304	138

Table 1. Continued

	substance	relative transport rate[b] (% of control)	$logD_{7.4}$[c]	MW[d] g × mol^{-1}	PSA[e] Å^2
	mesalazine	109 ± 11	−2.0	153	88
	tomoxetine	109 ± 11	1.5	255	22
	etoposide	110 ± 23	0.3	589	187
	probenecid	110 ± 27	−1.0	285	75
	nizatidine	110 ± 18	0.7	331	88
	prednisolone	110 ± 12	1.5	360	89
	chrysin	110 ± 13	2.8	254	71
	tetracycline[h]	110 ± 17	−2.6	444	181
	4-methylumbelliferone glucuronide	111 ± 21	−2.9	352	158
	medroxyprogesterone	111 ± 21	3.5	344	55
	cholic acid[h]	112 ± 13	1.7	409	99
	ritodrine	113 ± 11	0.6	287	79
	sulindac sulfone	113 ± 6	0.7	372	81
	sulfanitran	116 ± 18	0.9	335	123
	reduced L-glutathione[h]	116 ± 27	−5.9	307	165
	furosemide	118 ± 25	−0.8	331	123
borderline stimulators	ketoprofen	120 ± 11	−0.1	254	59
	nevirapine	121 ± 21	1.5	266	52
	17β-estradiol	123 ± 19	3.6	272	45
	progesterone	123 ± 20	3.9	314	38
	hydrocortisone	124 ± 9	1.6	362	89
	phenytoin	125 ± 11	2.1	252	62
	spironolactone	125 ± 12	2.9	417	67
	flutamide	126 ± 14	3.0	276	66
	methotrexate	130 ± 24	−4.8	454	217
	ibuprofen	130 ± 29	1.1	206	41
	mifepristone	134 ± 10	4.9	430	44
	pravastatin	135 ± 20	0.4	425	119
	warfarin	136 ± 22	1.1	308	58
	oxidized L-glutathione	136 ± 29	−6.8	613	330
	sparfloxacin	138 ± 7	−2.9	392	101
	testosterone	140 ± 15	3.3	288	42
	glimepiride	142 ± 11	2.8	491	119
stimulators	sulfinpyrazone	150 ± 15	−1.2	404	59
	budesonide	150 ± 24	2.3	431	87
	acetaminophen glucuronide	150 ± 16	−3.6	327	155
	sulindac	151 ± 33	0.3	356	62
	gliclazide	174 ± 19	−0.2	323	79
	mitoxantrone	175 ± 47	−2.6	444	166
	diclofenac	198 ± 20	1.4	296	54
	naringenin	207 ± 28	1.7	272	95
	nitrendipine	224 ± 25	3.4	360	116
	estrone-3-sulfate	300 ± 67	0.2	350	91
	glibenclamide	304 ± 66	2.7	494	110
	indomethacin	308 ± 23	0.2	358	78
	dehydroisoandrosterone-3-sulfate	395 ± 48	0.3	368	90

[a] Experimentally determined inhibition and stimulation of MRP2-mediated $E_{17}G$ transport is shown for the compounds in this study, along with important molecular descriptors. [b] Calculated as the ratio of the ATP-dependent $E_{17}G$ transport rate in the presence and absence of the test compound. Compounds that significantly decreased the ATP-dependent transport rate to less than 50% of the control were regarded as inhibitors ($n = 42$), and compounds that increased the transport rate by at least 50% were regarded as stimulators ($n = 13$). Only compounds with marginal effects on the $E_{17}G$ transport (±20% of the control; $n = 76$) were regarded as noninhibitors in the computational analysis to avoid bias from moderately inhibiting compounds (20–50% inhibition; $n = 43$) or moderately stimulating compounds (20–50% stimulation; $n = 17$). [c] Octanol–water partition coefficient at pH 7.4, calculated using ADMETPredictor version 2.4.4. [d] Molecular weight. [e] Polar surface area, calculated using MAREA version 3.02. [f] n.a.: not applicable. [g] Previously unknown MRP2 inhibitors. [h] Included in the test set used to validate the OPLS-DA model of MRP2 inhibition.

An additional analysis was performed to examine whether inhibitors that have also been reported to be substrates and which are thus likely to compete with $E_{17}G$ binding at the transport site were structurally different from other inhibitors. Inhibitors also shown to be substrates were on average less lipophilic than other inhibitors and also had a higher molecular weight and a larger polar surface area (Table 2).

Structural Characteristics of MRP2 Stimulators. To determine molecular characteristics important for stimulatory binding to MRP2, we also examined molecular properties separating stimulators from compounds that did not affect $E_{17}G$ transport. After variable selection, eight molecular descriptors were included in the final correlation. The relationship suggested that stimulators mainly differ from noninteracting compounds by a greater negative charge, larger number of functional groups involved in hydrogen bonding, lower lipophilicity, and smaller size. In fact, all stimulators found in this study carry at least one negative charge at physiological pH. Interestingly, the charge characteristics of the data set of stimulators were comparable to those reported for MRP2 substrates (Figure 3G), suggesting that the stimulating binding site(s) may be similar to the transport binding site.[22,28] All the experimentally determined MRP2 transport stimulators were correctly classified by the model, whereas 15 of the 75 noninteracting compounds were classified as stimulators. Notably, as many as 10 of these 15 compounds have, in assays optimized for studying stimulation,

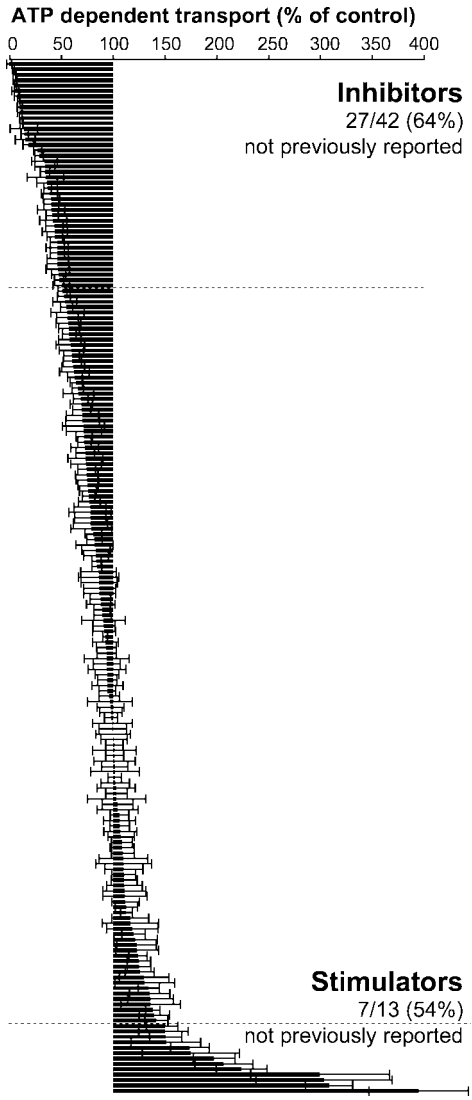

Figure 2. Identification of inhibitors and stimulators of MRP2-mediated $E_{17}G$ transport. $E_{17}G$ transport was measured in inverted membrane vesicles from MRP2-overexpressing Sf9 cells after incubation with 50 μM $E_{17}G$ with or without 80 μM of the test compound. Of the 191 test compounds, 42 (22%) inhibited MRP2-mediated $E_{17}G$ transport at this concentration, and 13 compounds (7%) mediated a significantly increased transport rate. A decrease in ATP-dependent transport rate of at least 50% was used as the cutoff for significant MRP2 inhibition, and an increase of at least 50% was regarded as significant stimulation. The data are presented as means ± S.E. ($n = 3$), with the compounds in the same order as in Table 1.

either been reported to be stimulators of MRP2-mediated transport or stimulation has been observed for highly structurally similar compounds.[22,29] The structural characteristics of the 13 stimulators in our study were thus in agreement with those of other stimulators reported in the literature.

Discussion

In this study, we used a global approach to explore the structural features determining MRP2 inhibition. A data set of 191 compounds representing the chemical space of oral drugs was investigated, resulting in the identification of 27 previously unknown MRP2 inhibitors. In total 22% of the investigated compounds inhibited MRP2-mediated $E_{17}G$ transport, a hit frequency about half that previously observed for the two other important ABC transporters BCRP (37%)[27] and P-gp (44%).[30] A large proportion (67%) of the MRP2 inhibitors also have affinity for P-gp or BCRP.[27,31–33] This indicates an overlapping but also narrower inhibitor space for MRP2 than for the two other major hepatic ABC transporters.

Inhibition of MRP2 can lead to toxic accumulation of drugs and bile acids in the liver, and the fact that many drugs interact with multiple transporters and drug-metabolizing enzymes increases the risk of serious adverse effects when parallel detoxification pathways are inhibited at the same time. To facilitate studies of the interplay between different transport mechanisms, we selected a reference data set mainly intended for studies of hepatic drug-transporter interaction, although also model compounds for CYP metabolism and liver toxicity were included (Figure 5). We believe that this data set will benefit global comparisons of drug affinity for liver transporters and also enable comparisons of different experimental and computational methods.

Notably, 10 out of the 14 FDA-recommended CYP inhibitors and substrates that were included in the reference data set also interact with one or more transporters, suggesting that transporters can be a confounding factor in CYP interaction studies. Similarly, overlap between hepatic uptake and efflux transporters (Figure 5) was observed in several cases; 9 of the 21 compounds in the reference data set reported as substrates or inhibitors of uptake transporters in the organic anion transporting polypeptide (OATP/SLCO) family were hits in the MRP2 assay. A similar overlap (6/20) was seen for the organic anion transporter (OAT1-5/SLC22A6-11) family. In contrast, only one of the 23 compounds with affinity for organic cation transporters (OCT1-3/SLC22A1-3) also interacted with MRP2, which was expected from the current understanding of interactions between organic anions and MRP2.[34,35] Consequently, anionic compounds that are dependent on transporters for both their entry into the hepatocyte and their efflux into bile may become trapped inside the cell when coadministered with MRP2 inhibitors, with a risk for intracellular accumulation and toxic effects. For example, hepatic uptake of the antibacterial drug rifampicin is mediated by the anion uptake transporters OATP1A2, 1B1, and 1B3.[36,37] Once inside the hepatocyte, rifampicin competes with endogenous MRP2 substrates for efflux, resulting in adverse effects such as hyperbilirubinemia, especially in patients with genetically compromised MRP2 function.[12,38] Similar adverse effects related to impaired lipid disposition have been reported for several of the new MRP2 inhibitors in our investigation.[38] A number of clinical trials have demonstrated elevated plasma levels of cholic acids after treatment with HIV protease inhibitors such as ritonavir and saquinavir,[39,40] both of which significantly inhibited MRP2-mediated transport in this study. We propose that inhibition of MRP2-mediated bile efflux leading to compensatory active or passive transport into the bloodstream by other transporters thus could be part of the explanation for the altered plasma levels.

The computational analysis identified lipophilicity and aromaticity as important molecular properties for MRP2 inhibition. This is similar to the picture seen for the related ABC transporter BCRP (ABCG2), where $\log D_{7.4}$ and polarizability, the latter describing electron delocalization in conjugated systems, were the most important molecular descriptors for differentiating between inhibitors and noninhibitors.[27,41] Another interesting observation is that the charge distribution among the identified MRP2 inhibitors clearly differs from that in substrates and stimulators. Almost one-third of the MRP2 inhibitors carry a positive charge at physiological pH, whereas substrates and stimulators are essentially neutral or negatively charged (Figure 3G). These differences support previous observations that MRP2 has a complex interaction pattern with

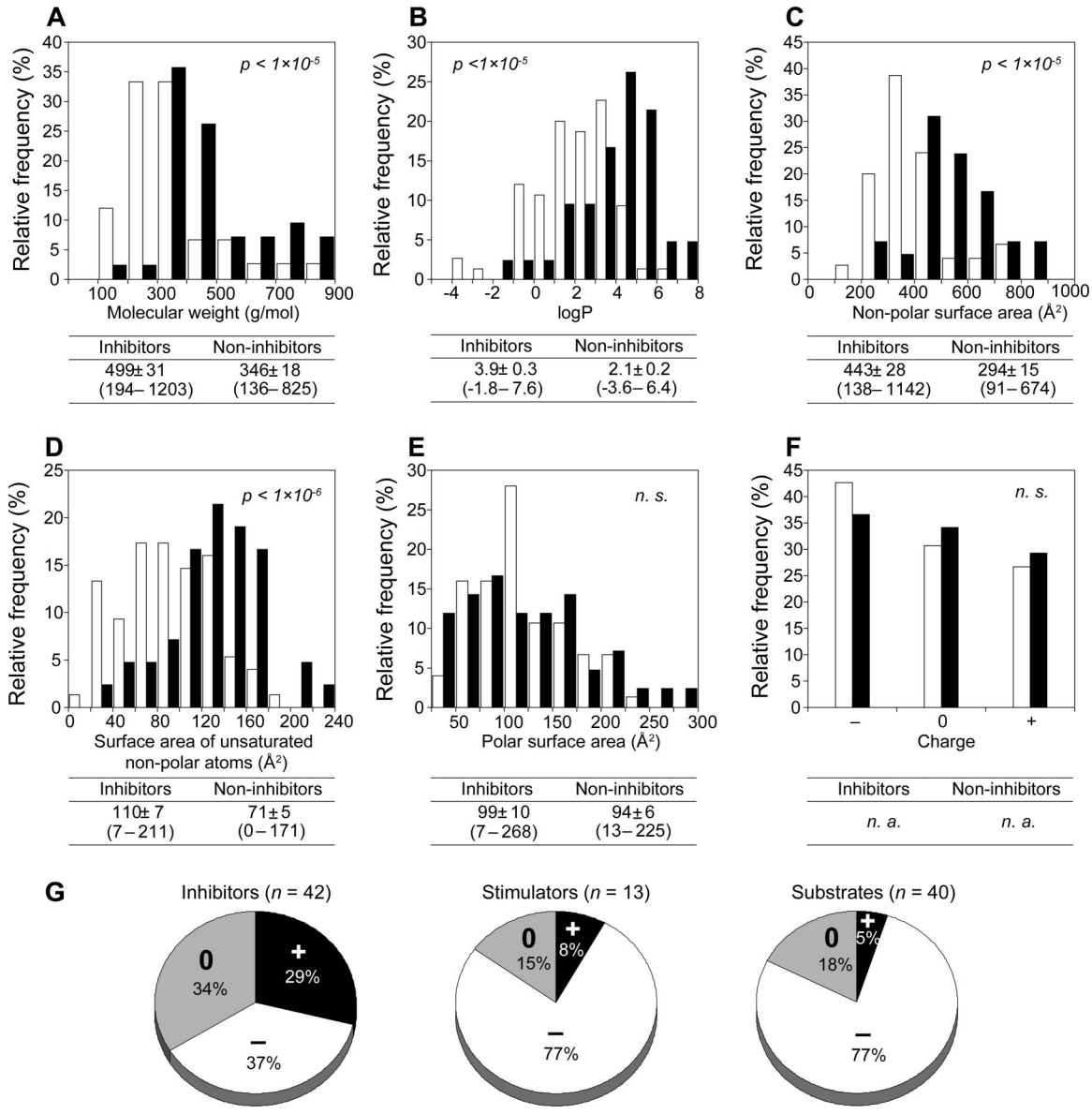

Figure 3. Physicochemical properties of MRP2 inhibitors and noninhibitors. The molecular descriptors represent the size (molecular weight, A), lipophilicity (octanol–water partition coefficient, B), hydrophobicity (surface area of nonpolar atoms, C), aromaticity (surface area of unsaturated nonpolar atoms, D), hydrogen bonding capacity (surface area of polar atoms, E), and major ionic species (charge, F). The closed bars denote the distributions of the MRP2 inhibitors, and the open bars denote the distributions of the noninhibitors. Below each graph the means ± SE of that physicochemical property are given for the inhibitors and noninhibitors, with the range of observed values within brackets. The differences between inhibitors and noninhibitors were statistically significant ($p < 0.01$) for the physicochemical properties depicted in A−D. (G) Distribution of molecular charge in MRP2 inhibitors, stimulators, and substrates. The relative frequency of compounds in which the dominating ionic species at pH 7.4 had positive (+), negative (−), or no charge (0) is shown for MRP2 inhibitors ($n = 42$) and stimulators ($n = 13$) in this study, along with the distribution in previously reported MRP2 substrates ($n = 40$).[32] Notably, all stimulators, including those with positive or neutral molecular net charge, carry at least one negative charge at physiologic pH. The stimulators also exhibit a charge distribution very similar to the MRP2 substrates. A more complex charge distribution with no clearly predominating net charge is observed for the MRP2 inhibitors.

several cooperative binding sites.[22,34] Based on the analysis of the physicochemical properties of the inhibitors, substrates, and stimulators we hypothesize that the inhibitors can be clustered into two groups, possibly binding to different sites in the transporters (Figure 6).

Most of the compounds with reported affinity for the MRP2 substrate transport site are relatively hydrophilic and are either negatively charged or cotransported as ion pairs with negatively charged glutathione (Figure 3G).[34,42–45] Membrane accumulation and passive permeability of such compounds are likely to be limited by charge–charge repulsion from the negatively charged polar head-groups of lipids in the inner membrane leaflet, and their cellular uptake is often mediated by membrane transporters.[7,14,31,36,37,44,46] Therefore, it is unlikely that the transporting site of MRP2 is situated within the membrane. Support for a cytosolic location of the transport binding site is obtained from studies of the closely related ABC transporter MRP1 (ABCC1), for which several amino acids in the cytosolic loops affect the substrate binding.[47] The fact that MRP1 and MRP2 share affinity for several anionic and conjugated substrates[47,48] indicates that the binding mechanism may be similar for these transporters. This similarity is further supported by that positively charged residues in the cytosol−membrane interfaces of the same transmembrane helices (TM6, 11, and 17) are important for transport in both MRPs.[47,49,50] The importance of amino acids

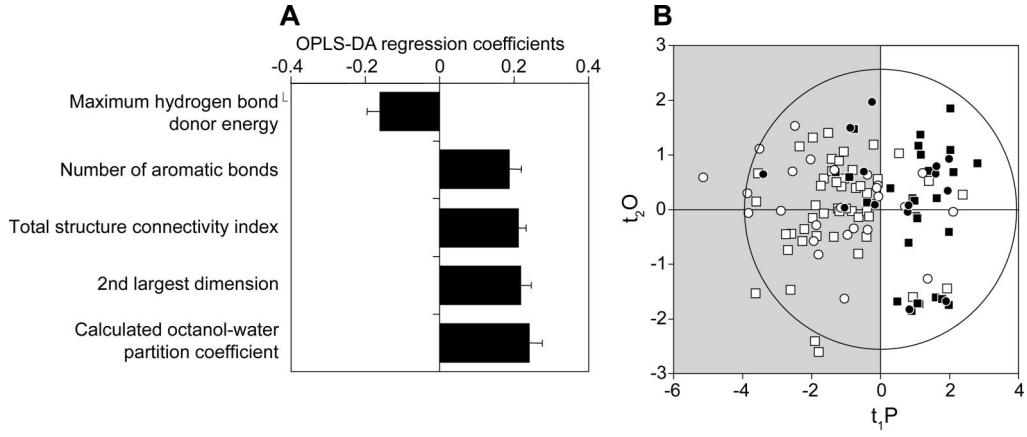

Figure 4. Prediction of MRP2 inhibition from five molecular descriptors. (A) The molecular descriptors included in the final model after stepwise exclusion of insignificant descriptors, as described in the Materials and Methods. The remaining molecular descriptors are related to lipophilicity (calculated octanol–water partition coefficient), size (second largest dimension, total structure connectivity index), aromaticity (number of aromatic bonds), and hydrogen bonding potential (maximum hydrogen bond donor energy). Descriptors with higher absolute coefficients have greater influence on the discriminant model. Positive coefficients mean that the descriptors have higher values in MRP2 inhibitors, whereas descriptors with negative coefficients have higher values in noninhibitors. (B) The orthogonal PLS discriminant analysis score plot showing the predictive (t_1P) and the first orthogonal (t_2O) principal component. Compounds in the shaded area are predicted to be noninhibitors. The closed symbols denote compounds experimentally determined to inhibit MRP2, and the open symbols denote noninhibitors. Compounds in the training set are shown as squares, and test set compounds (which were withheld from the model development, see Materials and Methods) are shown as circles. The model was capable of correctly classifying 86% of both the inhibitors and noninhibitors in the training set and 72% of the inhibitors and 71% of the noninhibitors in the test set.

Table 2. Physicochemical Differences between "Pure" MRP2 Inhibitors and MRP2 Inhibitors that are also Substrates[a]

molecular descriptor	transported inhibitors ($n = 9$)[b] mean values (median)	"pure" inhibitors ($n = 33$)[c] mean values (median)	difference
molecular weight ($g \times mol^{-1}$)	615 ± 40 (720)	470 ± 60 (414)	$p < 1 \times 10^{-5}$
$logD_{7.4}$	1.5 ± 0.5 (0.5)	3.2 ± 0.7 (3.6)	$p < 1 \times 10^{-5}$
polar surface area ($Å^2$)	152 ± 12 (139)	84 ± 19 (73)	$p < 1 \times 10^{-5}$

[a] The means ± SE are presented for each parameter. Median values are given within brackets. [b] Data supporting MRP2-mediated transport were obtained from the transporter database available from the University of Tokyo.[61] [c] Inhibitors that have not been reported as MRP2 substrates.

located in the cytosolic part of the protein indicates that substrates bind to this family of transporters directly from the intracellular compartment (A in Figure 6). Thus, inhibitors also reported as substrates are likely to interact with the cytosolic substrate binding site and competitively inhibit the transport.

Analogous to the charge distribution in MRP2 substrates, all compounds that stimulated transport in this study carry at least one negative charge at physiological pH (Figure 3G). This finding supports the statement that the transport stimulating binding site may have similar physicochemical properties to those of the transport binding site[22,28] and that it is likely to be located in the part of MRP2 facing the cytosol (B in Figure 6). Similar to the substrate and stimulatory binding sites, the ATP-binding sites of ABC transporters seem to favor interactions with negatively charged molecules, although this has only been studied for a few compounds, and the detailed characteristics of such interactions are yet to be discovered.[51,52]

The evident difference in charge distribution at physiological pH between inhibitors and other MRP2-interacting groups (Figure 3G) implies that the positively charged subset of MRP2 inhibitors forms a second group of inhibitors (Table 2). We hypothesize that this group of more lipophilic inhibitors can accumulate in the cell membrane[53] and interact with MRP2 in a fashion similar to those proposed for P-gp[31] and BCRP[27] (Table 2; C in Figure 6). Support for this hypothesis is obtained from that several of the more lipophilic, positively charged MRP2 inhibitors have also been reported to interact with P-gp or BCRP from within the plasma membrane.[27,31,53] However, whether these inhibitors interact with a binding site different from those proposed for substrates and stimulators remains to be determined, e.g. using site-directed mutagenesis.

In conclusion, despite the challenges imposed by the multiple drug binding sites in MRP2 and by our choice of a global data set spanning the chemical space of oral drug-like molecules, a predictive qualitative model for identification of MRP2 inhibitors was successfully developed. This model was capable of correctly classifying 86% of both the inhibitors and noninhibitors in the training set and 72% of the inhibitors and 71% of the noninhibitors in the test set and was based on easily interpreted molecular descriptors. We believe that classification models such as our MRP2 model can, in addition to shedding some light on the molecular mechanism of MRP2 inhibition, aid in flagging compounds with structural properties likely to increase the risk of MRP2-mediated hepatic drug interactions and toxicity in an early stage of the drug discovery process.

Materials and Methods

Selection of the Experimental Data Set, Including a Reference Data Set for Studies of Hepatic Transporters. One of the limitations of published studies of drug−transporter interactions to date is that the data sets of drug-like molecules have been narrow, covering only a small proportion of the structural drug space.[15–18] While this approach is useful for the establishment of quantitative structure−transport relationships, the predictivity of such models is limited to compounds from the same structural series. In this study, we therefore used a global modeling approach and included 191 compounds in the data set covering the chemical space of oral drugs.

As an integral part of this global data set, we highlighted a panel of 75 compounds that we propose can be used as a reference set

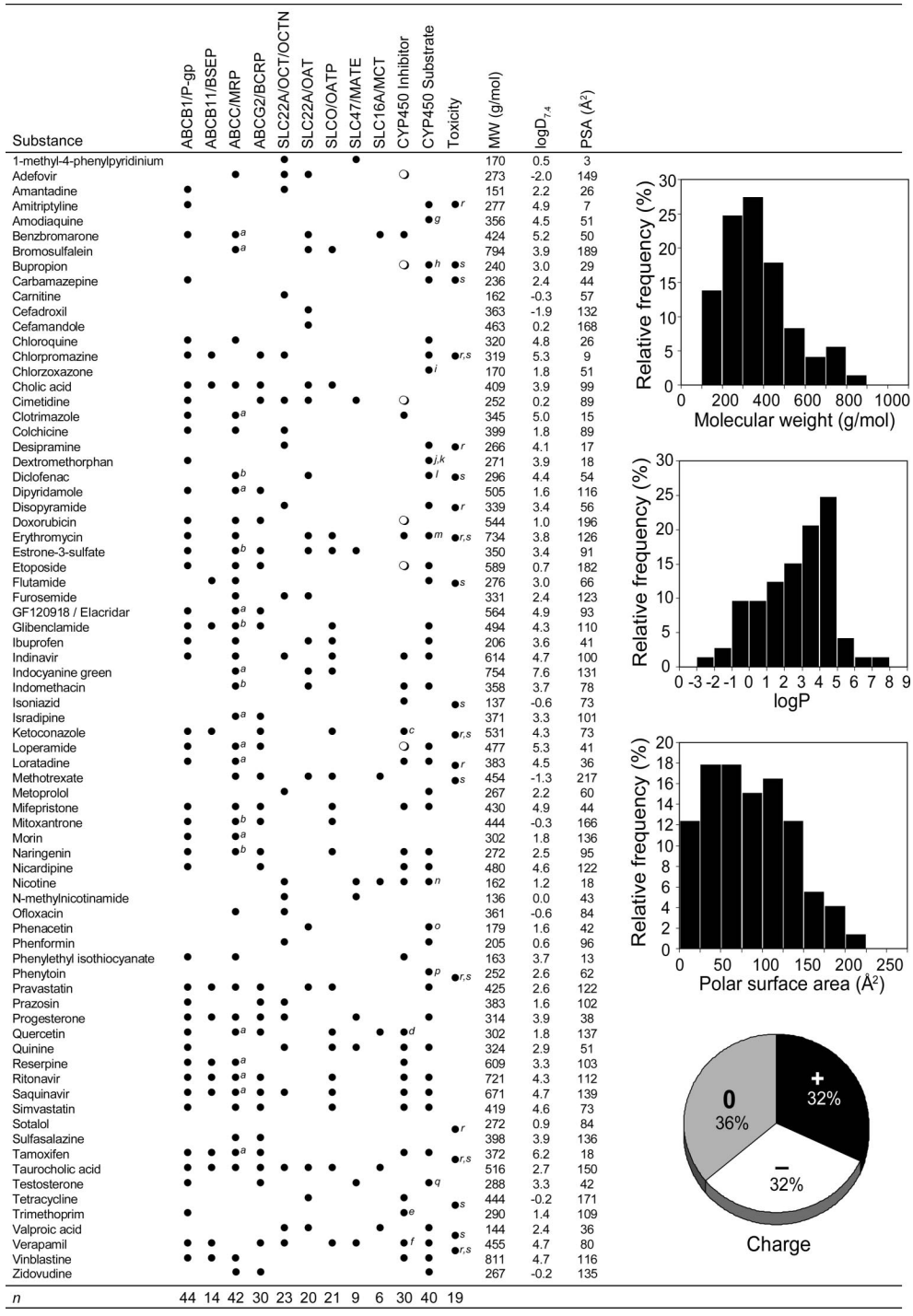

Figure 5. Affinity profile and physicochemical characteristics of the hepatic transporter reference data set. The 75 compounds were selected to be representative of the structural space of orally administered drugs and to have affinity for a panel of important hepatic transporters and metabolic enzymes. For transporters, closed symbols denote that the compound has been reported to (i) reduce transport with at least 50% at an inhibitor concentration not exceeding 100 μM or (ii) be a transported substrate. For CYP enzymes, closed symbols denote that the compound has been reported to (i) reduce metabolism with at least 50% at an inhibitor concentration not exceeding 20 μM or (ii) be a metabolized substrate. Open symbols denote compounds which have been reported to reduce metabolism with at least 50% at inhibitor concentrations in the range 20–100 μM. Note that missing symbols do not necessarily imply a lack of affinity but can also result from missing data in the literature. The PubMed literature search was performed using the search string "<compound name> AND <transporter name>" or "<compound name> AND (CYP or "cytochrome P450")". Examples of compounds associated with toxicity are marked according to reviews of hepatic or hERG-mediated toxicity, see table footnotes for references. Footnotes to Figure 5: [a] MRP2 inhibitor in this study. [b] MRP2 stimulator in this study. [c] FDA preferred CYP3A4/5 inhibitor. [d] FDA preferred CYP2C8 inhibitor. [e] FDA accepted CYP2C8 inhibitor. [f] FDA accepted CYP3A4/5 inhibitor. [g] FDA accepted CYP2C8 substrate. [h] FDA preferred CYP2B6 substrate. [i] FDA preferred CYP2E1 substrate. [j] FDA accepted CYP3A4/5 substrate. [k] FDA preferred CYP2D6 substrate. [l] FDA preferred CYP2C9 substrate. [m] FDA accepted CYP3A4/5 substrate. [n] FDA preferred CYP2A6 substrate. [o] FDA preferred CYP1A2 substrate. [p] FDA accepted CYP2C9 substrate. [q] FDA preferred CYP3A4/5 substrate. [r] Associated with hERG toxicity according to Zünkler, *Pharmacol. Ther.* **2006**, *112*, 12–37 or de Bruin et al., *Eur. Heart J.* **2005**, *26*, 590–597. [s] Associated with hepatic toxicity according to Navarro and Senior, *New Engl. J. Med.* **2006**, *354*, 731–739 or Lee, *New Engl. J. Med.* **2003**, *349*, 474–485.

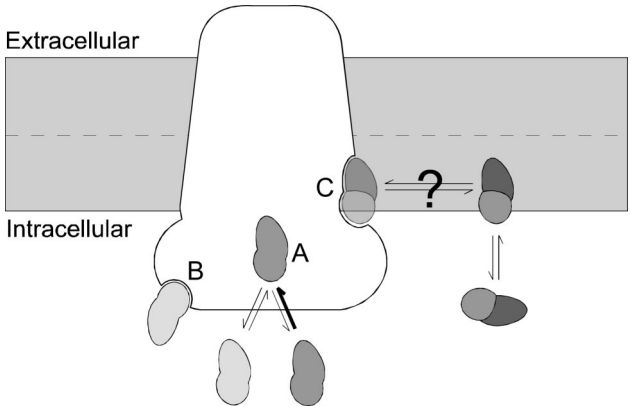

Figure 6. Proposed drug binding sites in MRP2. Depending on its physicochemical properties, a drug can interact with MRP2 at several different sites. Transported inhibitors such as bromosulfalein and glycyrrhizinic acid can compete for binding to the cytosolic transport site (A), which is more likely for negatively charged and hydrophilic compounds. Compounds that stimulate MRP2 transport, such as dehydroisoandrosterone-3-sulfate, can bind to a second cytosolic binding site (B) similar to the transport site. We further suggest that lipophilic cationic inhibitors, such as thioridazine and terfenadine, are unlikely to bind to the two cytosolic binding sites because of charge repulsion, and might, after partitioning to the plasma membrane[31,53] interact with a third binding site accessible from the lipid bilayer (C).

for drug-transporter interaction studies. Since many drugs interact with several transporters and metabolic enzymes, such a data set has the potential to provide information about the complex interplay between different mechanisms. The data set primarily focuses on transporters known to influence hepatic drug disposition, but many of these are also important in other organs, including the intestine, liver, and blood−brain barrier.[2,4,54]

First, we identified a data set comprising 220 compounds that have been reported to interact with both efflux transporters from the ABC family, including P-glycoprotein (ABCB1/P-gp), BSEP (ABCB11), MRP1-8 (ABCC1-6, 10-11), and BCRP (ABCG2), and uptake transporters from the SLC family, including the organic cation transporters (SLC22A1-3/OCT1-3), organic anion transporters (SLC22A6-11/OAT1-5 and SLCOs/OATPs), multidrug and toxin extrusion transporters (SLC47/MATE), and monocarboxylate transporters (SLC16A1-7/MCTs). Compounds commonly used as markers for important drug-metabolizing cytochrome P450 enzymes (CYP1A2, 2B6, 2C8/9/19, 2D6, 2E1, and 3A4/5/7) were also included, as were a set of compounds known to cause hepatotoxicity and another set known to cause hERG receptor-mediated cardiotoxicity.

From the initial selection, 75 compounds were chosen for inclusion in the final transporter reference data set (Figure 5). The compounds were selected specifically to cover the chemical space of oral drugs, while at the same time covering interactions with the entire panel of uptake and efflux transporters, CYP enzymes, and toxicity issues. The significant reduction in the size of the data set was made possible by the inclusion of compounds with overlapping affinities for several transporters and enzymes.

Furthermore, because we had previously observed a large overlap in inhibitor affinities among different ABC transporters, 90 additional compounds with reported ABC transporter affinity were included in the data set, along with a set of 26 compounds with unknown transporter affinity, selected from an in-house database of drugs from the Physician's Desk Reference.[38] The solubilities of the selected compounds were predicted using an in-house computational solubility model and compounds with solubility below the selected assay concentration were replaced with compounds that exhibited sufficient solubility and that were located in close proximity to each of the excluded compounds in the chemical drug space. Compounds with predicted solubility close to the assay concentration were evaluated using literature values, and were kept in the data set only if sufficiently soluble according to the literature data.

In summary, 191 endogenous or drug-like compounds were included in this study (for SMILES, see Supporting Information, Table S2). These compounds comprised three groups: (A) a structurally diverse reference set for hepatic transporter affinity studies ($n = 75$), (B) compounds with a reported affinity for ABC transport proteins ($n = 90$), and (C) compounds ($n = 26$) selected from an in-house database of drugs from the Physician's Desk Reference.[38]

Substances. Amantadine, amiloride, captopril, carbamazepine, chlorprothixene, chlorzoxazone, erythromycin, fenofibrate, flupenthixol, glipizide, hydrochlorthiazide, prednisone, sulindac, terfenadine, tetracycline, and tinidazole were kind gifts from Dr. Anders Karlén (Dept. of Medicinal Chemistry, Uppsala University, Sweden). Ko143 was a kind gift from Dr. Gerrit-Jan Koomen (Van't Hoff Institute for Molecular Sciences, University of Amsterdam, Netherlands). GF120918 was kindly provided by GlaxoSmithKline (Stevenage, U.K.). MK571 was purchased from A.G. Scientific (San Diego, CA) and astemizole from MP Biomedicals (Eschwege, Germany). [^{3}H]-Estradiol-17β-D-glucuronide ($E_{17}G$) was obtained from PerkinElmer (Waltham, MA). All other compounds were purchased from Sigma-Aldrich, St. Louis, MO, or International Laboratory Limited (San Bruno, CA), and were of at least 95% purity.

MRP2 Transport Assay. Inverted membrane vesicles from Sf9 cells overexpressing human MRP2 were used throughout the investigation, and $E_{17}G$ was used as a model substrate for MRP2 transport.[55] Statistical experimental design as implemented in Modde version 7.0 (Umetrics, Umeå, Sweden) was used to optimize the experimental parameters of the $E_{17}G$ transport assay. Six experimental parameters were varied in the design (Supporting Information, Table S1), including (i) the amount of membrane vesicles per well, (ii) the $E_{17}G$ concentration, (iii) the ratio of radiolabeled to unlabeled $E_{17}G$, (iv) the lag time between thawing the vesicle solution and starting the incubation, (v) the incubation time, and (vi) the concentration of MK571, which was used as a positive inhibition control.[23] Five levels of each parameter were considered using a two-layered onion design,[56] resulting in a total of 33 experiments designed to cover the widest possible extent of parameter combinations (Supporting Information, Table S1).

The experiments were performed in a 96-well plate format using a rapid filtration technique modified from Ishikawa et al.[57] Briefly, the transport buffer consisting of 10 mM Tris-HCl solution (pH 7.4), supplemented with 250 mM sucrose, 10 mM $MgCl_2$, and 10 mM phosphocreatine was preheated to 37 °C. MRP2 membrane vesicles were quickly thawed from −85 to 37 °C and diluted in the transport buffer to a final concentration of 0.4 μg/μL. Substrate and inhibitor solutions were prepared from 10 mM DMSO stock solutions and radiolabeled substrate was added to each well separately. The transport was initiated by the addition of ATP and creatine kinase at a final concentration of 5 mM and 90 U/mL, respectively. The vesicle solution was then incubated at 37 °C for 5 to 20 min using 300 rpm orbital shaking. All experiments were performed in duplicate, along with negative controls in which the ATP and creatine kinase solution were substituted by 5 mM AMP. The transport was stopped by adding 200 μL ice cold stop solution (10 mM Tris-HCl solution (pH 7.4) supplemented with 250 mM sucrose and 0.1 M NaCl), and the reaction mixture was immediately filtered through a 96-well glass filter plate with a pore size of 0.65 μm (Millipore, Bedford, MA). The filters were washed five times with 200 μL of ice cold stop solution, dried for 1.5 h at 37 °C, and transferred to scintillation vials containing 3 mL of Ultima Gold scintillation cocktail (PerkinElmer, Shelton, CT). The radioactivity was measured in a 1900CA TRICARB liquid scintillation counter (Canberra Packard Instruments, Downers Grove, IL). Disintegrations per minute were related to molar transport rates using standard samples of [^{3}H]-$E_{17}G$ diluted in assay solution. The ATP-dependent $E_{17}G$ transport rate was calculated by subtracting the negligible (~0.25%) transport rate in vesicles incubated with AMP from the rate in ATP-incubated vesicles.

Nonlinear regression (Prism version 4.02, GraphPad, San Diego, CA) was used to determine Michaelis–Menten kinetic parameters

from initial transport rates determined in a concentration range of 10 to 300 μM, according to eq 1

$$V = \frac{V_{max} \times [S]^{\gamma}}{K_m + [S]^{\gamma}} \quad (1)$$

where V_{max} is the maximal transport rate, [S] is the $E_{17}G$ concentration, K_m is the $E_{17}G$ concentration at which $V = 0.5 \times V_{max}$, and γ is the Hill coefficient.

Inhibition Assay. A statistical experimental design process was used to find assay parameter combinations resulting in both maximal ATP-dependent transport rates and maximal inhibitory effect of the MRP inhibitor MK571 (Supporting Information; Table S1). A membrane vesicle concentration corresponding to 10 μg membrane protein was selected, and the final substrate concentration was set to 50 μM $E_{17}G$, spiked with 85 nM (0.1 μCi) radiolabeled $E_{17}G$. This concentration was selected to minimize the effect of transport stimulation previously observed at low $E_{17}G$ concentrations.[22,34] The results of this process indicated that long incubation times improved the assay resolution, and an incubation time of 10 min was therefore selected, which was well within the range of linear transport (Figure 1A). The experimental design results suggested that high inhibitor concentrations were favorable but that increasing lag times between thawing the vesicles and the start of the experiment did not significantly improve the assay. A standard inhibitor concentration of 80 μM was chosen, which is in the vicinity of the $E_{17}G$ transport K_m. A lag time of 5 min was used to ensure that the temperature of the membrane vesicle preparation was consistent at the initiation of all experiments.

Because of the risk of solubility issues for some of the investigated compounds at the 80 μM concentration, DMSO was used as a cosolvent. The effect of DMSO on the $E_{17}G$ transport was shown to be negligible for final DMSO concentrations up to 0.5% (data not shown). Consequently, the test compounds were diluted from 16 mM DMSO stock solutions to a final concentration of 80 μM (0.5% DMSO). All experiments were performed in triplicate with negative controls in which ATP and creatine kinase solution were substituted by 5 mM AMP. Each experiment included positive transport controls, in which the vesicles were incubated with $E_{17}G$ without the addition of an inhibitor. Positive inhibition controls using the MRP inhibitor MK571 were also included on each plate, resulting in an interday variability of 3%.

The ratio of the ATP-dependent $E_{17}G$ transport rate in the presence and absence of the test compound was used as the end point for inhibitory effects. Compounds that significantly decreased the ATP-dependent transport to less than 50% of the control were regarded as inhibitors. The chosen cutoff level resulted in maximal statistical significance when the Student's *t*-test was used to compare the modulation of the transport rate by compounds above and below the cutoff level.

Computational Modeling. Molecular structures obtained from SciFinder Scholar 2006 (American Chemical Society, Washington, DC) were used as the input for 3D structure generation using Corina version 3.0 (Molecular Networks, Erlangen, Germany). A total of 669 molecular decriptors, representing mainly the molecular size, flexibility, connectivity, polarity, charge, and hydrogen bonding potential of the molecules, were calculated from the 3D structures using DragonX version 3.0 (Talete, Milano, Italy), ADMETPredictor version 1.2.4 (SimulationsPlus, Lancaster, CA), and HYBOT (MOLPRO-2001, TimTec, Newark, DE). The static-free molecular surface areas for each atom type were calculated using the in-house software MAREA version 3.02, as described previously.[58,59] After removal of descriptors with zero variance, 240 descriptors were used as a starting point for development of the model.

The data set division was performed in two steps. First, the data set was divided into two groups based on their experimentally determined MRP2 inhibitory effect. Compounds inhibiting the transport by at least 50% were regarded as inhibitors ($n = 42$). Only compounds with marginal effects on the transport (±20% compared to control) were included in the noninhibitor group ($n = 76$) to avoid bias to the model from moderately inhibiting compounds (20–50% inhibition; $n = 43$). Compounds resulting in increased $E_{17}G$ transport ($n = 30$) were also excluded from the MRP2 inhibition model. The compounds were then divided into a training set used for model development and a test set used to validate the predictivity of the final model. A representative test set was selected using ChemGPS descriptions of the molecules.[60] In ChemGPS, the position of a compound in the drug-like chemical space is determined using principal components calculated from descriptors of their chemical structure. Structural diversity was maximized by selecting compounds from throughout ChemGPS space, resulting in a test set with structural features representative of the compounds in the training set (Supporting Information, Figure S1). Two-thirds of the compounds in each activity group (28 inhibitors and 51 noninhibitors) were included in the training set, and the remaining one-third (14 inhibitors and 25 noninhibitors) were included in the test set.

Orthogonal partial least-squares projection to latent structures discriminant analysis (OPLS-DA), as implemented in Simca-P version 11.5 (Umetrics, Umeå, Sweden), was used to derive multivariate classification models for separating MRP2 inhibitors from noninhibitors. The influence on the model of the different sizes of the inhibitor and noninhibitor groups was balanced by replication of the inhibitor entries in the data set. To avoid bias in the models, all replicates of a molecule were removed simultaneously during the cross-validation procedure. The models were optimized by a variable selection procedure in which groups of molecular descriptors that did not contain information relevant to the problem (i.e., noise) were removed in a stepwise manner. Descriptors were kept outside the model if removing them resulted in a statistically improved model, based on the classification accuracy for the training set. The statistical validity of the models was tested using a random permutation test, in which the order of the response variable was randomly changed 100 times. All presented models collapsed to subzero cross-validated coefficients of determination (Q^2) when the response variables were permutated, demonstrating that they were describing the response variables rather than noise.

Acknowledgment. This work was supported by the Swedish Research Council (Grant 9478), the Knut and Alice Wallenberg Foundation, the Swedish Foundation for Strategic Research, the Swedish Fund for Research without Animal Experiments, and the Swedish Animal Welfare Agency.

Supporting Information Available: Parameters optimized in the statistical experimental design, SMILES codes for all compounds in the data set, and a figure of the investigated data set projected in the chemical space of registered oral drugs. This material is available free of charge via the Internet at http://pubs.acs.org.

References

(1) Borst, P.; Elferink, R. O. Mammalian ABC transporters in health and disease. *Annu. Rev. Biochem.* **2002**, *71*, 537–592.
(2) Hilgendorf, C.; Ahlin, G.; Seithel, A.; Artursson, P.; Ungell, A. L.; Karlsson, J. Expression of thirty-six drug transporter genes in human intestine, liver, kidney, and organotypic cell lines. *Drug Metab. Dispos.* **2007**, *35*, 1333–1340.
(3) Nies, A. T.; Keppler, D. The apical conjugate efflux pump ABCC2 (MRP2). *Pflugers Arch.* **2007**, *453*, 643–659.
(4) Nishimura, M.; Naito, S. Tissue-specific mRNA expression profiles of human ATP-binding cassette and solute carrier transporter superfamilies. *Drug Metab. Pharmacokinet.* **2005**, *20*, 452–477.
(5) Hulot, J. S.; Villard, E.; Maguy, A.; Morel, V.; Mir, L.; Tostivint, I.; William-Faltaos, D.; Fernandez, C.; Hatem, S.; Deray, G.; Komajda, M.; Leblond, V.; Lechat, P. A mutation in the drug transporter gene ABCC2 associated with impaired methotrexate elimination. *Pharmacogenet. Genomics* **2005**, *15*, 277–285.
(6) Shitara, Y.; Sugiyama, Y. Pharmacokinetic and pharmacodynamic alterations of 3-hydroxy-3-methylglutaryl coenzyme A (HMG-CoA) reductase inhibitors: Drug−drug interactions and interindividual differences in transporter and metabolic enzyme functions. *Pharmacol. Ther.* **2006**, *112*, 71–105.

(7) Sasaki, M.; Suzuki, H.; Ito, K.; Abe, T.; Sugiyama, Y. Transcellular transport of organic anions across a double-transfected Madin-Darby canine kidney II cell monolayer expressing both human organic anion-transporting polypeptide (OATP2/SLC21A6) and multidrug resistance-associated protein 2 (MRP2/ABCC2). *J. Biol. Chem.* **2002**, *277*, 6497–6503.

(8) Keitel, V.; Nies, A. T.; Brom, M.; Hummel-Eisenbeiss, J.; Spring, H.; Keppler, D. A common Dubin-Johnson syndrome mutation impairs protein maturation and transport activity of MRP2 (ABCC2). *Am. J. Physiol.* **2003**, *284*, G165–G174.

(9) Isley, W. L. Hepatotoxicity of thiazolidinediones. *Expert Opin. Drug Saf.* **2003**, *2*, 581–586.

(10) Jaeschke, H.; Gores, G. J.; Cederbaum, A. I.; Hinson, J. A.; Pessayre, D.; Lemasters, J. J. Mechanisms of hepatotoxicity. *Toxicol. Sci.* **2002**, *65*, 166–176.

(11) Tang, W. Drug metabolite profiling and elucidation of drug-induced hepatotoxicity. *Expert Opin. Drug Metab. Toxicol.* **2007**, *3*, 407–420.

(12) Corpechot, C.; Ping, C.; Wendum, D.; Matsuda, F.; Barbu, V.; Poupon, R. Identification of a novel 974C-->G nonsense mutation of the MRP2/ABCC2 gene in a patient with Dubin-Johnson syndrome and analysis of the effects of rifampicin and ursodeoxycholic acid on serum bilirubin and bile acids. *Am. J. Gastroenterol.* **2006**, *101*, 2427–2432.

(13) Smitherman, P. K.; Townsend, A. J.; Kute, T. E.; Morrow, C. S. Role of multidrug resistance protein 2 (MRP2, ABCC2) in alkylating agent detoxification: MRP2 potentiates glutathione S-transferase A1–1-mediated resistance to chlorambucil cytotoxicity. *J. Pharmacol. Exp. Ther.* **2004**, *308*, 260–267.

(14) Chen, C.; Mireles, R. J.; Campbell, S. D.; Lin, J.; Mills, J. B.; Xu, J. J.; Smolarek, T. A. Differential interaction of 3-hydroxy-3-methylglutaryl-coa reductase inhibitors with ABCB1, ABCC2, and OATP1B1. *Drug Metab. Dispos.* **2005**, *33*, 537–546.

(15) Hirono, S.; Nakagome, I.; Imai, R.; Maeda, K.; Kusuhara, H.; Sugiyama, Y. Estimation of the three-dimensional pharmacophore of ligands for rat multidrug-resistance-associated protein 2 using ligand-based drug design techniques. *Pharm. Res.* **2005**, *22*, 260–9.

(16) Lai, Y.; Xing, L.; Poda, G. I.; Hu, Y. Structure-activity relationships for interaction with multidrug resistance protein 2 (ABCC2/MRP2): The role of torsion angle for a series of biphenyl-substituted heterocycles. *Drug Metab. Dispos.* **2007**, *35*, 937–945.

(17) Ng, C.; Xiao, Y. D.; Lum, B. L.; Han, Y. H. Quantitative structure−activity relationships of methotrexate and methotrexate analogues transported by the rat multispecific resistance-associated protein 2 (rMrp2). *Eur. J. Pharm. Sci.* **2005**, *26*, 405–413.

(18) Chang, G. Retraction of "Structure of MsbA from Vibrio cholera: A multidrug resistance ABC transporter homolog in a closed conformation" [*J. Mol. Biol.* (2003) *330*, 419–430]. *J. Mol. Biol.* **2007**, *369*, 596.

(19) Williamson, G.; Aeberli, I.; Miguet, L.; Zhang, Z.; Sanchez, M. B.; Crespy, V.; Barron, D.; Needs, P.; Kroon, P. A.; Glavinas, H.; Krajcsi, P.; Grigorov, M. Interaction of positional isomers of quercetin glucuronides with the transporter ABCC2 (cMOAT, MRP2). *Drug Metab. Dispos.* **2007**, *35*, 1262–1268.

(20) As an example, the crystal structure of the bacterial transporter MsbA from Vibrio Cholera with Protein Data Bank access number 1pf4 was recently retracted because of erroneous interpretation of both the structure and the protein topology.[18] A recently published homology model of MRP2 that used this structure as a template may consequently lead to erroneous conclusions.[19].

(21) Bodo, A.; Bakos, E.; Szeri, F.; Varadi, A.; Sarkadi, B. Differential modulation of the human liver conjugate transporters MRP2 and MRP3 by bile acids and organic anions. *J. Biol. Chem.* **2003**, *278*, 23529–23537.

(22) Zelcer, N.; Huisman, M. T.; Reid, G.; Wielinga, P.; Breedveld, P.; Kuil, A.; Knipscheer, P.; Schellens, J. H.; Schinkel, A. H.; Borst, P. Evidence for two interacting ligand binding sites in human multidrug resistance protein 2 (ATP binding cassette C2). *J. Biol. Chem.* **2003**, *278*, 23538–23544.

(23) Gekeler, V.; Ise, W.; Sanders, K. H.; Ulrich, W. R.; Beck, J. The leukotriene LTD4 receptor antagonist MK571 specifically modulates MRP associated multidrug resistance. *Biochem. Biophys. Res. Commun.* **1995**, *208*, 345–352.

(24) Rule Discovery System version 2.5.1 (Compumine, Uppsala, Sweden) was used to develop decision trees for discriminating between MRP2 inhibitors and non-inhibitors. The same molecular descriptors and dataset division were used as for the OPLS-DA model. However, the decision tree methodology was not suited for this particular problem, as evident from the poor predictivity of the models (<50%).

(25) Gombar, V. K.; Polli, J. W.; Humphreys, J. E.; Wring, S. A.; Serabjit-Singh, C. S. Predicting P-glycoprotein substrates by a quantitative structure−activity relationship model. *J. Pharm. Sci.* **2004**, *93*, 957–968.

(26) Penzotti, J. E.; Lamb, M. L.; Evensen, E.; Grootenhuis, P. D. A computational ensemble pharmacophore model for identifying substrates of P-glycoprotein. *J. Med. Chem.* **2002**, *45*, 1737–1740.

(27) Matsson, P.; Englund, G.; Ahlin, G.; Bergström, C. A. S.; Norinder, U.; Artursson, P. A global drug inhibition pattern for the human ABC transporter BCRP (ABCG2). *J. Pharmacol. Exp. Ther.* **2007**, *323*, 19–30.

(28) Borst, P.; Zelcer, N.; van de Wetering, K.; Poolman, B. On the putative co-transport of drugs by multidrug resistance proteins. *FEBS Lett.* **2006**, *580*, 1085–1093.

(29) Gerk, P. M.; Li, W.; Megaraj, V.; Vore, M. Human multidrug resistance protein 2 transports the therapeutic bile salt tauroursodeoxycholate. *J. Pharmacol. Exp. Ther.* **2007**, *320*, 893–899.

(30) Matsson, P.; Pedersen, J. M.; Norinder, U.; Bergström, C. A. S.; Artursson, P. Comparison and prediction of inhibitors of the three major human ATP-binding cassette transporters P-gp, BCRP and MRP2, *manuscript in preparation*, 2008.

(31) Gatlik-Landwojtowicz, E.; Äänismaa, P.; Seelig, A. Quantification and characterization of P-glycoprotein−substrate interactions. *Biochemistry* **2006**, *45*, 3020–3032.

(32) Ozawa, N.; Shimizu, T.; Morita, R.; Yokono, Y.; Ochiai, T.; Munesada, K.; Ohashi, A.; Aida, Y.; Hama, Y.; Taki, K.; Maeda, K.; Kusuhara, H.; Sugiyama, Y. Transporter database, TP-Search: A web-accessible comprehensive database for research in pharmacokinetics of drugs. *Pharm. Res.* **2004**, *21*, 2133–2134.

(33) Polli, J. W.; Wring, S. A.; Humphreys, J. E.; Huang, L.; Morgan, J. B.; Webster, L. O.; Serabjit-Singh, C. S. Rational use of in vitro P-glycoprotein assays in drug discovery. *J. Pharmacol. Exp. Ther.* **2001**, *299*, 620–628.

(34) Bakos, E.; Evers, R.; Sinko, E.; Varadi, A.; Borst, P.; Sarkadi, B. Interactions of the human multidrug resistance proteins MRP1 and MRP2 with organic anions. *Mol. Pharmacol.* **2000**, *57*, 760–768.

(35) Jedlitschky, G.; Keppler, D. Transport of leukotriene C4 and structurally related conjugates. *Vitam. Horm.* **2002**, *64*, 153–184.

(36) Cui, Y.; König, J.; Keppler, D. Vectorial transport by double-transfected cells expressing the human uptake transporter SLC21A8 and the apical export pump ABCC2. *Mol. Pharmacol.* **2001**, *60*, 934–943.

(37) Vavricka, S. R.; Van Montfoort, J.; Ha, H. R.; Meier, P. J.; Fattinger, K. Interactions of rifamycin SV and rifampicin with organic anion uptake systems of human liver. *Hepatology* **2002**, *36*, 164–172.

(38) *Physicians' Desk Reference*, 61st ed.; Medical Economics Data: Montvale, New Jersey, 2007.

(39) Manfredi, R.; Chiodo, F. Disorders of lipid metabolism in patients with HIV disease treated with antiretroviral agents: Frequency, relationship with administered drugs, and role of hypolipidaemic therapy with bezafibrate. *J. Infect.* **2001**, *42*, 181–188.

(40) Periard, D.; Telenti, A.; Sudre, P.; Cheseaux, J. J.; Halfon, P.; Reymond, M. J.; Marcovina, S. M.; Glauser, M. P.; Nicod, P.; Darioli, R.; Mooser, V. Atherogenic dyslipidemia in HIV-infected individuals treated with protease inhibitors. The Swiss HIV Cohort Study. *Circulation* **1999**, *100*, 700–705.

(41) Zhang, S.; Yang, X.; Coburn, R. A.; Morris, M. E. Structure−activity relationships and quantitative structure activity relationships for the flavonoid-mediated inhibition of breast cancer resistance protein. *Biochem. Pharmacol.* **2005**, *70*, 627–639.

(42) Cui, Y.; König, J.; Buchholz, J. K.; Spring, H.; Leier, I.; Keppler, D. Drug resistance and ATP-dependent conjugate transport mediated by the apical multidrug resistance protein, MRP2, permanently expressed in human and canine cells. *Mol. Pharmacol.* **1999**, *55*, 929–937.

(43) Evers, R.; de Haas, M.; Sparidans, R.; Beijnen, J.; Wielinga, P. R.; Lankelma, J.; Borst, P. Vinblastine and sulfinpyrazone export by the multidrug resistance protein MRP2 is associated with glutathione export. *Br. J. Cancer* **2000**, *83*, 375–383.

(44) Matsushima, S.; Maeda, K.; Kondo, C.; Hirano, M.; Sasaki, M.; Suzuki, H.; Sugiyama, Y. Identification of the hepatic efflux transporters of organic anions using double-transfected Madin-Darby canine kidney II cells expressing human organic anion-transporting polypeptide 1B1 (OATP1B1)/multidrug resistance-associated protein 2, OATP1B1/multidrug resistance 1, and OATP1B1/breast cancer resistance protein. *J. Pharmacol. Exp. Ther.* **2005**, *314*, 1059–1067.

(45) Van Aubel, R. A.; Koenderink, J. B.; Peters, J. G.; Van Os, C. H.; Russel, F. G. Mechanisms and interaction of vinblastine and reduced glutathione transport in membrane vesicles by the rabbit multidrug resistance protein Mrp2 expressed in insect cells. *Mol. Pharmacol.* **1999**, *56*, 714–719.

(46) Romsicki, Y.; Sharom, F. J. The membrane lipid environment modulates drug interactions with the P-glycoprotein multidrug transporter. *Biochemistry* **1999**, *38*, 6887–6896.

(47) Bakos, E.; Homolya, L. Portrait of multifaceted transporter, the multidrug resistance-associated protein 1 (MRP1/ABCC1). *Pflugers Arch.* **2007**, *453*, 621–641.

(48) Keppler, D.; Cui, Y.; König, J.; Leier, I.; Nies, A. Export pumps for anionic conjugates encoded by MRP genes. *Adv. Enzyme Regul.* **1999**, *39*, 237–246.

(49) Ito, K.; Suzuki, H.; Sugiyama, Y. Charged amino acids in the transmembrane domains are involved in the determination of the substrate specificity of rat Mrp2. *Mol. Pharmacol.* **2001**, *59*, 1077–1085.
(50) Ryu, S.; Kawabe, T.; Nada, S.; Yamaguchi, A. Identification of basic residues involved in drug export function of human multidrug resistance-associated protein 2. *J. Biol. Chem.* **2000**, *275*, 39617–39624.
(51) Conseil, G.; Baubichon-Cortay, H.; Dayan, G.; Jault, J. M.; Barron, D.; Di Pietro, A. Flavonoids: A class of modulators with bifunctional interactions at vicinal ATP- and steroid-binding sites on mouse P-glycoprotein. *Proc. Natl. Acad. Sci. U.S.A.* **1998**, *95*, 9831–9836.
(52) de Wet, H.; McIntosh, D. B.; Conseil, G.; Baubichon-Cortay, H.; Krell, T.; Jault, J. M.; Daskiewicz, J. B.; Barron, D.; Di Pietro, A. Sequence requirements of the ATP-binding site within the C-terminal nucleotide-binding domain of mouse P-glycoprotein: Structure−activity relationships for flavonoid binding. *Biochemistry* **2001**, *40*, 10382–10391.
(53) Seelig, A.; Gatlik-Landwojtowicz, E. Inhibitors of multidrug efflux transporters: Their membrane and protein interactions. *Mini-Rev. Med. Chem.* **2005**, *5*, 135–151.
(54) Shitara, Y.; Horie, T.; Sugiyama, Y. Transporters as a determinant of drug clearance and tissue distribution. *Eur. J. Pharm. Sci.* **2006**, *27*, 425–446.
(55) Keppler, D.; Leier, I.; Jedlitschky, G. Transport of glutathione conjugates and glucuronides by the multidrug resistance proteins MRP1 and MRP2. *Biol. Chem.* **1997**, *378*, 787–791.
(56) Eriksson, L. A., T.; Beck, B.; Fox, T.; Johansson, E.; Kriegl, J. M. Onion design and its application to a pharmaceutical QSAR problem. *J. Chemom.* **2004**, *18*, 188–202.
(57) Ishikawa, T.; Müller, M.; Klunemann, C.; Schaub, T.; Keppler, D. ATP-dependent primary active transport of cysteinyl leukotrienes across liver canalicular membrane. Role of the ATP-dependent transport system for glutathione S-conjugates. *J. Biol. Chem.* **1990**, *265*, 19279–19286.
(58) Matsson, P.; Bergström, C. A.; Nagahara, N.; Tavelin, S.; Norinder, U.; Artursson, P. Exploring the role of different drug transport routes in permeability screening. *J. Med. Chem.* **2005**, *48*, 604–613.
(59) Palm, K.; Stenberg, P.; Luthman, K.; Artursson, P. Polar molecular surface properties predict the intestinal absorption of drugs in humans. *Pharm. Res.* **1997**, *14*, 568–571.
(60) Oprea, T. I.; Gottfries, J. Chemography: The art of navigating in chemical space. *J. Comb. Chem.* **2001**, *3*, 157–166.
(61) Omote, H.; Al-Shawi, M. K. Interaction of transported drugs with the lipid bilayer and P-glycoprotein through a solvation exchange mechanism. *Biophys. J.* **2006**, *90*, 4046–4059.

JM7015683